PNAS RESEARCH ARTICLE | CHEMISTRY ANTHROPOLOGY

Disentangling the chemistry of Australian plant exudates from a unique historical collection

Rafaella Georgiou[a,b,1], Rachel S. Popelka-Filcoff[c,d,1,2], Dimosthenis Sokaras[e], Victoria Beltran[f], Ilaria Bonaduce[g], Jordan Spangler[d], Serge X. Cohen[a], Roy Lehmann[d], Sylvain Bernard[h], Jean-Pascal Rueff[b,i], Uwe Bergmann[j,k,2], and Loïc Bertrand[a,b,l,2]

Edited by Catherine Patterson, Getty Conservation Institute, Los Angeles, CA; received September 25, 2021; accepted March 8, 2022, by Editorial Board Member Natasha V. Raikhel

For thousands of years, the unique physicochemical properties of plant exudates have defined uses in material culture and practical applications. Native Australian plant exudates, including resins, kinos, and gums, have been used and continue to be used by Aboriginal Australians for numerous technical and cultural purposes. A historic collection of well-preserved native Australian plant exudates, assembled a century ago by plant naturalists, gives a rare window into the history and chemical composition of these materials. Here we report the full hierarchical characterization of four genera from this collection, *Xanthorrhoea*, *Callitris*, *Eucalyptus*, and *Acacia*, from the local elemental speciation, to functional groups and main molecular markers. We use high-resolution X-ray Raman spectroscopy (XRS) to achieve bulk-sensitive chemical speciation of these plant exudates, including insoluble, amorphous, and cross-linked fractions, without the limitation of invasive and/or surface specific methods. Combinatorial testing of the XRS data allows direct classification of these complex natural species as terpenoid, aromatic, phenolic, and polysaccharide materials. Differences in intragenera chemistry was evidenced by detailed interpretation of the XRS spectral features. We complement XRS with Fourier-transform infrared (FT-IR) spectroscopy, gas chromatography–mass spectrometry (GC-MS), and pyrolysis–GC-MS (Py-GC-MS). This multimodal approach provides a fundamental understanding of the chemistry of these natural materials long used by Aboriginal Australian peoples.

plant exudates | resins | Australia | spectroscopy | cultural heritage

Significance

For millennia, Aboriginal Australian peoples have used the extraordinary physicochemical properties of plant exudates from practical applications to cultural expression. We employ state-of-the-art spectroscopy to characterize the molecular compositions of well-preserved, native Australian plant exudates (*Xanthorrhoea*, *Callitris*, *Eucalyptus*, and *Acacia*) from a historic collection assembled over a century ago. This work demonstrates the benefits of X-ray Raman spectroscopy for the analysis of these complex natural systems. It provides key information for a broader understanding of their terpenoid, aromatic, phenolic, and polysaccharide composition and subsequent chemical classification. It complements Fourier-transform infrared and pyrolysis–gas chromatography–mass spectrometry by allowing bulk-sensitive analysis in a fully noninvasive manner and probes molecular features which remain silent in these commonly employed analyses.

For millennia, societies have empirically utilized the physicochemical properties of plant exudates including resins, kinos, and gums and implemented them in practical applications and cultural expression (1–3). Indigenous Australians across the continent developed technologies over thousands of years for processing the naturally occurring organic materials, maximizing their effective use for each purpose (e.g., hafting stone tools to handles, paint binders, and priming layers on bark paintings) (4–14). To change or enhance their properties, specific exudates were often mixed with ochre and other materials (e.g., fibers) (6, 15–17). Plant exudates continue to be incorporated in a variety of contemporary cultural contexts (13). For example, Aboriginal Australian artists may choose to use traditional plant exudate binders over synthetic materials such as acrylic or oil binders to intentionally connect artworks to their local landscape, tradition, and culture (13, 15).

Only a few chemical characterization studies of natural Australian plant exudates have been reported in the context of raw exudates and on cultural heritage materials. Blee et al. (5) have examined samples including *Xanthorrhoea tateana*, *Xanthorrhoea semiplana*, and an *Acacia* gum of an unknown species belonging to the ethnobotany collection of the South Australian Museum (SAM) by Fourier-transform infrared (FT-IR) and chemometric techniques. The authors were able to differentiate native Australian resins and identified probable candidates used for hafted stone knives (5). Reeves et al. reanalyzed the same three samples and also characterized known Australian and European materials of different chemical classes by pyrolysis–gas chromatography–mass spectrometry (Py-GC-MS) with subsequent statistical analysis (10). Analyses of the same materials by different methods demonstrated consistent results, e.g., the identification of the C–C ring stretching by FT-IR and the identification of phenolic groups by Py-GC-MS for the *Xanthorrhoea* genus. Both papers find that the *Acacia* and *Xanthorrhoea* samples can be distinguished from the other samples by characteristics in each genus. Bradshaw (12) employed GC-MS to chemically characterize six ethnographic resins belonging to the Pitt Rivers Museum collected one hundred years ago. Matheson et al. (6) analyzed a collection of both raw plant materials and resins from Queensland Museum objects, by FT-IR and GC-MS. While not identifying the major components of the species examined from the

Copyright © 2022 the Author(s). Published by PNAS. This article is distributed under Creative Commons Attribution-NonCommercial-NoDerivatives License 4.0 (CC BY-NC-ND).

[1] R.G. and R.S.P.-F. contributed equally to this work.

[2] To whom correspondence may be addressed. Email: rachel.popelkafilcoff@unimelb.edu.au, ubergmann@wisc.edu, or loic.bertrand@ens-paris-saclay.fr.

This article contains supporting information online at https://www.pnas.org/lookup/suppl/doi:10.1073/pnas.2116021119/-/DCSupplemental.

Published May 26, 2022.

Downloaded from https://www.pnas.org by 82.142.7.94 on May 26, 2022 from IP address 82.142.7.94.

raw plant materials and artifacts, the authors were able to assign *Xanthorrhoea*, *Triodia*, and *Erythrophleum chlorostachys* resins on archaeological objects to their plant resin counterparts by matching elution times in GC-MS and spectral features in attenuated total reflectance (ATR) FT-IR (6).

At the turn of the 20th century, a group of unknown naturalists assembled an extensive and comprehensive collection of plant exudates sampled across Australia, carefully annotating location information, with most collected from about 1876 to 1905. These samples have been stored up to the present in labeled brown glass jars. Further details and storage conditions of the collection are lost to time; however, it is assumed that the individual jars have been kept together and therefore experienced the same conditions over the decades. The first documentation of the collection was in the laboratories at the Art Gallery of South Australia. When these laboratories were closed in the late 1980s, the collection was transferred and held in the South Australian state forensic laboratory (Forensic Science South Australia [FSSA]) until the early 2000s. Subsequently, the collection was bequeathed to Flinders University by former scientists at FSSA, Paul Kirkbride and Paul Pigou, with the intention for further research about this unique time capsule of samples. This exceptional collection offers a rare glimpse into well-preserved plant exudates of major cultural and technological interest used both by Aboriginal Australian and non-Indigenous Australian peoples.

Here we elucidate the chemistry of native Australian plant exudates from four distinct genera (*Xanthorrhoea*, *Callitris*, *Eucalyptus*, and *Acacia*) preserved in this historic collection (*SI Appendix*, Table S1). While some genera are uniquely from Australia or Oceania and have properties that are not seen in other parts of the globe (*Xanthorrhoea*, *Callitris*, and *Eucalyptus*), species of *Acacia* are found worldwide (18). Although from distinct geographical origins, exudates from *Callitris* have been noted for their chemical similarities to sandarac resin from the *Tetraclinis articulata* tree from northern Africa. Similarly, exudates from Australian *Acacia* have parallels from other *Acacia* species that produce gum Arabic (*Acacia senegal* now known as *Senegalia senegal*) (19). Despite almost exclusive characterization of gum Arabic, the vast majority of over a thousand *Acacia* (wattle) species worldwide are found in Australia, and very few have been chemically characterized. This genus represents many of the general classes of plants that produce exudates in Australia (1) and those used in cultural applications and scientific research (6, 15).

X-ray Raman spectroscopy (XRS) is an element-specific hard X-ray technique (20, 21) that provides atomic-level chemical speciation information for light elements such as carbon and oxygen. Similar to electron energy loss spectroscopy (EELS), XRS is an energy-loss form of X-ray absorption near-edge structure (XANES) spectroscopy (also known as near-edge X-ray absorption fine structure) (22). Using hard X-rays, the technique overcomes the limitations of conventional XANES for the study of these organic samples related to the short penetration depth of soft X-rays at the carbon (285 eV) and oxygen (540 eV) K edges. As XRS is a bulk-sensitive probe, it does not require special sample treatment and/or environment. It can be applied in a noninvasive manner to probe bulk carbon speciation (millimeter scale) in complex organic systems, including valuable heritage samples (23, 24). XRS has also been successfully employed as a three-dimensional imaging probe to study natural heritage organic samples to determine organic signatures and trace their evolution through time (24).

We combine XRS and FT-IR, which provides molecular specificity from identification of major functional groups (approximately proportional to their concentration), with thermally assisted hydrolysis and methylation (THM) using tetramethylammonium hydroxide (TMAH) coupled to GC-MS (TMH/GC-MS), which characterizes a material at the molecular level, through the mass spectrometric determination of its products of thermal decomposition. Moreover, GC-MS was used after hydrolysis and silylation for the characterization of polysaccharides (*Acacia* samples), which are hydrolyzable polymers.

We show that straightforward and sensitive characterization and discrimination of the complex organic compounds is attained using XRS in a noninvasive manner. This work is an in-depth XRS-based statistical intercomparison of complex natural samples. Our application of XRS and complementary techniques provides an atomic-level understanding of the chemical speciation of the plant exudates in this rare collection. XRS can be applied for the chemical characterization of samples without being invasive and can be considered as a powerful tool for the chemical characterization and fine spectroscopic analysis of solid organic materials.

Main Spectroscopic Properties of the Plant Exudates

XRS carbon K-edge (Fig. 1) and oxygen K-edge (*SI Appendix*, Fig. S2) spectra were collected for a variety of plant species and genera. The XRS process is based on the inelastic scattering of a high-energy incident photon, $\hbar\omega_1$, which excites a core electron to a vacant higher-energy molecular orbital, while the excess of energy is released with a scattered photon, $\hbar\omega_2$ (21, 25, 26). Spectral decomposition of the normalized background-corrected XRS signal was performed as described (*SI Appendix*, *XRS Data Reduction*). XRS is able to provide a unique chemical fingerprint for each of the plant genera under study; thus, it can be considered as a reliable noninvasive tool for their discrimination. XRS data interpretation was based on an important corpus of work on carbon K-edge XANES and EELS. A database of inner shell excitation spectra obtained by EELS, gathering a large number of carbon and oxygen K-edge spectra, is provided by Hitchcock and Mancini (27). Thermally assisted hydrolysis and methylation (THM) using tetramethylammonium hydroxide (TMAH) coupled on line to GC-MS (TMH/GC-MS) were collected to provide structural information of the *Xanthorrhoea*, *Callitris*, and *Eucalyptus* samples. For the analysis of the *Acacia* samples (polysaccharide materials), we employed GC-MS analysis after hydrolysis and derivatization, rather than analytical pyrolysis, since establishing a relationship among the saccharide composition and the pyrolytic profile is not straightforward. FT-IR assignments were based on handbooks (28–30) and specific studies cited therein. FT-IR (*SI Appendix*, Fig. S3), GC-MS, and THM/GC-MS data (Fig. 2 and *SI Appendix*, Figs. S4–S14 and Table S7) were used to assist in the interpretation of the XRS features and the accurate assignment of the core electron transitions in various functional groups.

***Xanthorrhoea* Resins.** *Xanthorrhoea* resins are phenolic resins, comprising polyflavanoids, chalcones, flavanones, and free aromatic acids (31, 32). Compared to all other plant exudates studied, *Xanthorrhoea* species exhibit the highest amount of aromatic and/or olefinic carbon, which can be considered as a defining feature of the species (Fig. 1*A* and *SI Appendix*, Table S6). The XRS carbon K-edge spectra are dominated by the presence of an intense peak at 285.5 eV attributed to the 1s–π^* transitions in aromatic/olefinic groups (Fig. 1*A*). The presence of aromatic groups is confirmed by the FT-IR high-intensity sharp peaks centered at 1,602, 1,512, and 1,444 cm^{-1}

Downloaded from https://www.pnas.org by 82.142.7.94 on May 26, 2022 from IP address 82.142.7.94.

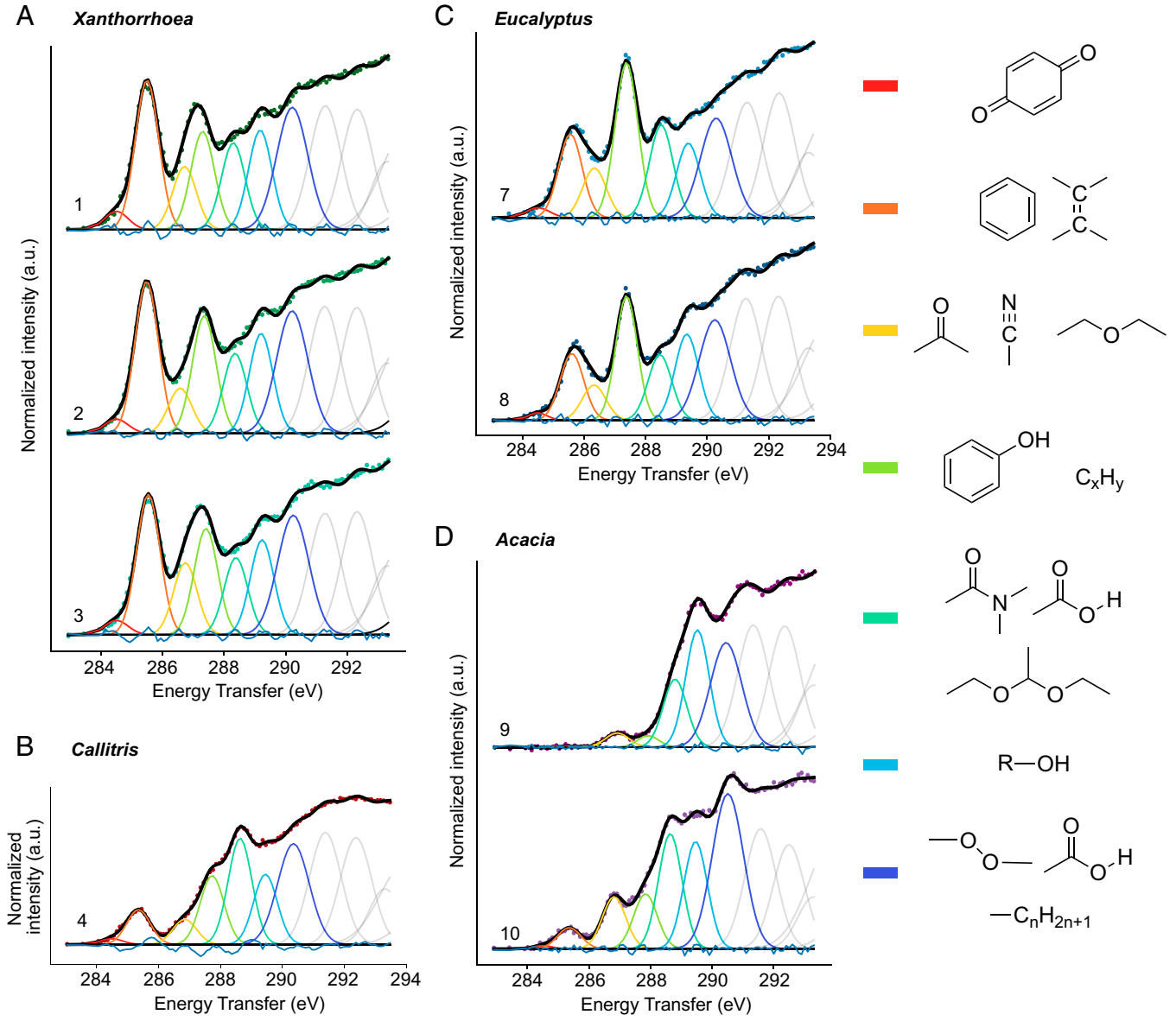

Fig. 1. XRS carbon K-edge spectra decomposition. (*A*) 1, *X. arborea*; 2, *X. semiplana* ssp. *tateana*; 3, *X. semiplana*. (*B*) 4, *C. calcarata*. (*C*) 7, white mallee; 8, *E. largiflorens*. (*D*) 9, *Acacia* sp.; 10, *A. bakeri*. For comparison of the samples' chemistry in a semiquantitative way, we performed a decomposition of the normalized spectra. The centers of Gaussians correspond to core electron transitions at specific functional groups as reported in the literature of soft X-rays absorption and/or EELS studies (SI Appendix, Table S2). For the interpretation of the XRS data only the transitions of core electrons to bound unoccupied states (i.e., preedge transitions) up to approximately 291.5 eV were used. Above that limit, there is contribution from highly delocalized excited states (i.e., 1s–σ* transitions) and overlapping contribution of Feshbach resonances.

attributed to C=C stretching (*SI Appendix*, Fig. S3*C*) and by the chemical structure of all the compounds identified in the pyrograms (*SI Appendix*, Figs. S4–S6). The FT-IR band centered at 1,636 cm^{-1}, attributed to C=C stretching of nonaromatic C=C bonds, is in agreement with the presence of p-coumaric acid and chalcones (*SI Appendix*, Figs. S4 and S5). Their presence is higher in *Xanthorrhoea arborea*, while for *X. semiplana* and *X. semiplana* ssp. *tateana* the 1,636 cm^{-1} band is less noticeable in agreement with pyrolytic profiles (*SI Appendix*, Fig. S3). The weak intensity FT-IR peak observed at 3,023 cm^{-1} is attributed to the C–H stretching in alkene groups (*SI Appendix*, Fig. S3*B*).

The XRS feature at 287.3 to 287.4 eV (center of fitted Gaussian 4 varies among the *Xanthorrhoea* species; *SI Appendix*, Table S4) is attributed to the 1s–π* transitions in phenols (Ar–OH) and to a lesser extent to 1s–3p/σ* transitions in aliphatic groups (C_xH_y) (Fig. 1*A*) (35). This is confirmed by the weak FT-IR bands in the 3,000 to 2,800 cm^{-1} region corresponding to C–H antisymmetric and symmetric stretch of CH_3 and CH_2 groups (*SI Appendix*, Fig. S3*B*). The FT-IR bands centered at 1,337 and 1,205 cm^{-1}, linked to the O–H deformation/C–OH stretching, are observable in all *Xanthorrhoea* species (*SI Appendix*, Fig. S3*C*). The broad signal in the 3,550 to 3,250 cm^{-1} region is attributed to –OH stretching (*SI Appendix*, Fig. S3*A*). This is in agreement with the detection of compounds ascribable to the pyrolysis and methylation of polyflavanoids, chalcones, and flavanones (*SI Appendix*, Figs. S4 and S5) (31, 32). Upon reaction with TMAH, hydroxyl groups are converted into methyl groups.

The Gaussian 3 fitted at 286.6 to 286.7 eV (the center varies among *Xanthorrhoea* species; *SI Appendix*, Table S4) is tentatively assigned to 1s–π* transitions in ketones ($R_2C{=}O$) (Fig. 1*A*). Oxygen 1s–π* excitation in carbonyl groups (C=O) (Gaussian 1 centered at 531.1 to 531.5 eV) is observed at the XRS oxygen

Downloaded from https://www.pnas.org by 82.142.7.94 on May 26, 2022 from IP address 82.142.7.94.

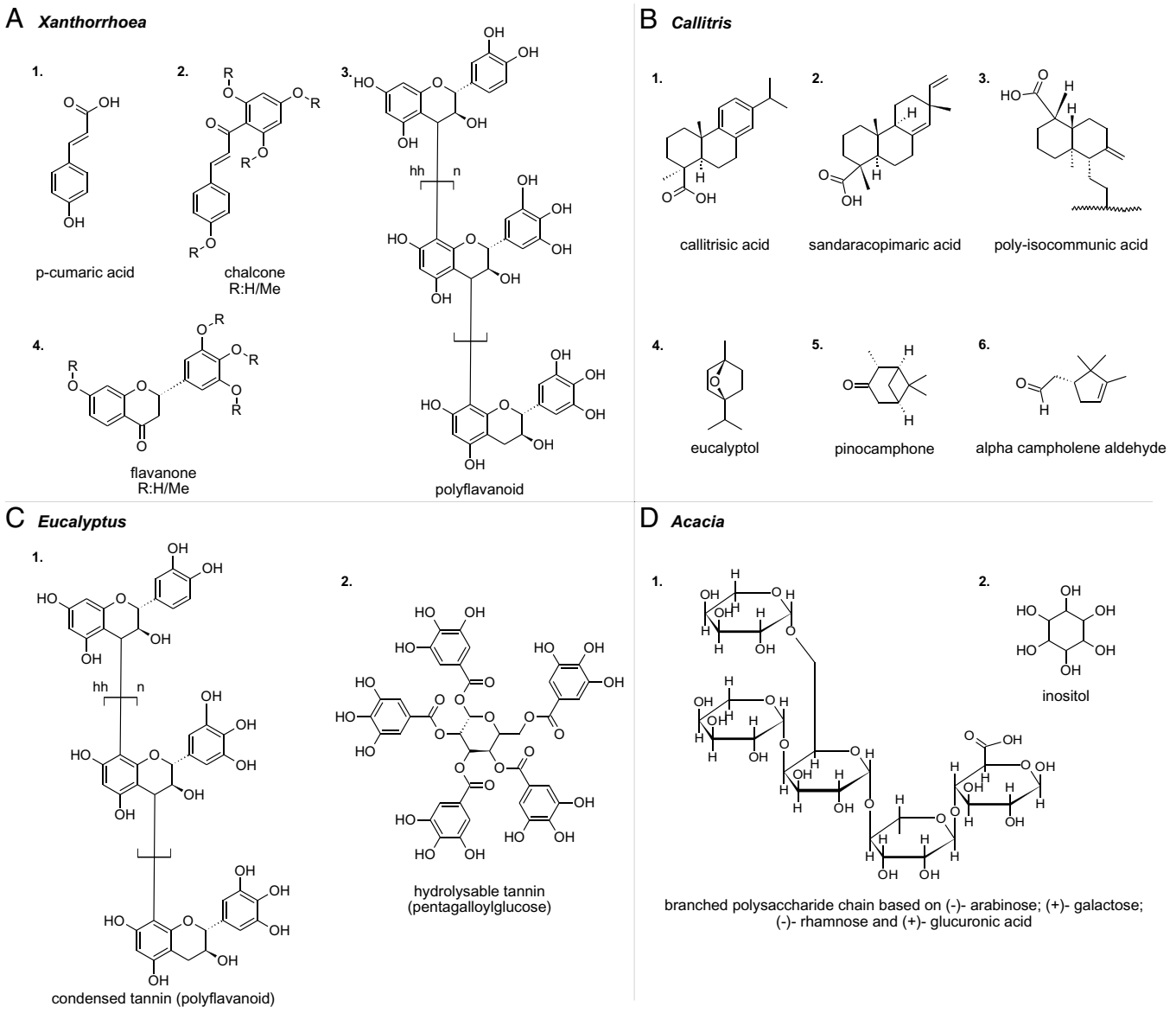

Fig. 2. (*A*) Main constituents of the *Xanthorrhoea* exudates based on the main pyrolysis products and information retrieved from the literature on the resin macromolecular structure (refs. 31, 32 and references therein). The exact position of methoxyl groups cannot be established given the analytical approach adopted in this study. (*B*) Main constituents of the *Callitris* exudates based on the main pyrolysis products. (*C*) Main constituents of the *Eucalyptus* exudates based on the main pyrolysis products and information retrieved from the literature on the kino macromolecular structure (33, 34). (*D*) Branched polysaccharide chain built with (–)- arabinose; (+)- galactose; (–)- rhamnose, and (+)- glucuronic acid, which are the monosaccharide constituents found in the *Acacia* gums. The polysaccharide structure cannot be determined with the techniques used in this study, and it is not reported in the literature. Inositol is only detected in *Acacia* sp.

K-edge spectra (*SI Appendix*, Fig. S2*A*). The spectral features attributed to ketones is in agreement with the presence of both chalcones and flavanones (Fig. 2*A*; aromatic ketone compounds). FT-IR spectra exhibit a small shoulder around 1,670 cm^{-1} that could be related to the C=O of aromatic ketones, which appears at lower wavelengths than aliphatic ketones, in agreement with the presence of aromatic acids and flavonoids, due to the conjugation (*SI Appendix*, Figs. S3*C*, S4 and S5) (36). The XRS feature centered at 289.2 eV is attributed to the 1s–3p/σ^* electronic transitions in hydroxyl groups (R–OH) which are present in polyflavanoids (Fig. 1*A* and *SI Appendix*, Table S6) (35).

***Callitris* Resins.** *Callitris* exudates are diterpenoid resins (37). The XRS carbon K-edge spectrum of *Callitris calcarata* is characterized by a main peak at 288.7 eV assigned to the 1s–π^* electronic transitions in carboxyl groups (–COOH) (Fig. 1*B*). The presence of carboxyls in the sample are confirmed by the strong broad feature of the FT-IR spectrum centered at 1,695 cm^{-1} attributed to C=O stretching of carboxylic acids (*SI Appendix*, Fig. S3*A*), the band around 3,450 cm^{-1} related to O–H stretching and the peak at 1,236 cm^{-1} linked to the C–OH stretching/O–H deformation of the OH groups (*SI Appendix*, Fig. S3*C*). The XRS oxygen K-edge spectra of *Callitris* species confirm as well the abundance of carboxylic acids. Compared to all the other genera, the spectra exhibit a higher intensity peak centered at 532.1 eV assigned to the oxygen C=O 1s–π^* transitions in carboxyls (–COOH) while the feature centered at 535.2 eV is attributed to the oxygen O–H 1s–π^* transitions in carboxyl groups (–COOH) (38) (*SI Appendix*, Fig. S2*B*). This is in agreement with the Py-GC-MS data: pimarane (methyl sandaracopimarate and methyl isopimarate) and abietane (methyl callitrisate) diterpenoid acids, as well as their hydroxyl derivatives dominate the pyrograms (*SI Appendix*, Figs. S7–S9). Signals ascribable to the pyrolysis of polycommunic acid, obtained by the polymerization

Downloaded from https://www.pnas.org by 82.142.7.94 on May 26, 2022 from IP address 82.142.7.94.

of communic acids, a diterpenoid with a labdane skeleton, are also well visible in the pyrograms (*SI Appendix*, Fig. S9) (39). In particular, the detection of iso-communic acid in the pyrograms suggests that the polymers are based on poly(iso)communic acid. More details are reported in *SI Appendix*.

The XRS peak at 285.4 eV corresponds to 1s–π^* transitions in aromatic or olefinic groups (C=C) (Fig. 1*B*). The presence of low-intensity bands at 1,610 and 1,497 cm^{-1} attributed to the C=C stretching in aromatic compounds indicates the low aromaticity of the *Callitris* species (*SI Appendix*, Fig. S3*C*) and can be related to callitrisic acid, which possesses an aromatic carbon ring. *C. calcarata* is the resin with the lowest content of callitrisic acid. The FT-IR band centered at 1,644 cm^{-1} attributed to the C=C stretching is linked to the presence of nonaromatic C=C bonds. The band at 3,080 cm^{-1} linked to the C–H stretching from the C=C moieties confirms the existence of these structures (*SI Appendix*, Fig. S3*B*). Olefinic groups are found in the pimarane diterpenoid acids (*SI Appendix*, Fig. S7). The three resins also contain nonnegligible amounts of monoterpenoids, some of which present C=C bonds (*SI Appendix*, Fig. S10). The low-intensity XRS feature centered at 286.7 eV is possibly attributed to 1s–π^* electronic transitions in ketone groups (Fig. 1*B*). The FT-IR shoulder around 1,726 cm^{-1} is attributed to the C=O stretching in ketones, and the 1,236 cm^{-1} band is attributed to the O–H bending in alcohols (*SI Appendix*, Fig. S3*C*). Ketone carbonyl groups are found in 7-oxocallitrisic acid as well as some monoterpenoids (i.e., pinocamphone, isopiperitenone, and alpha campholene aldehyde, *SI Appendix*, Fig. S10). The 1,236 cm^{-1} band assigned to the O–H bending in alcohols (*SI Appendix*, Fig. S3*C*) is in agreement with the detection of hydroxyl derivatives of both pimarane and abietane acids in the pyrograms (*SI Appendix*, Figs. S7 and S9). The low-intensity FT-IR bands linked to the presence of ketone and alcohol groups, together with the detection by THM/GC-MS of relatively high amounts of monoterpenoids and small amounts of oxidation products, indicate a low aging degree of the *Callitris* resins.

The broad XRS feature in the region 287.3 to 288 eV, centered at 287.6 eV, is attributed to the 1s–3p/σ^* of aliphatic groups (Fig. 1*B*); their presence is confirmed by the strong intensity peaks of CH_2 and CH_3 antisymmetric and symmetric stretch in the 3,000 to 2,800 cm^{-1} region of the FT-IR spectrum (*SI Appendix*, Fig. S3*B*). The presence of these groups is confirmed by the bands around 1,467 cm^{-1} (–CH_2–) and around 1,384 cm^{-1} (deformation of CH_3 and CH_2 groups) (*SI Appendix*, Fig. S3*C*). The high content of CH_2 and CH_3 groups is in agreement with the terpenoid nature of the resin.

***Eucalyptus* Kino.** *Eucalyptus* kinos are wood exudates rich in tannins, which are polyphenolic compounds. The XRS carbon K-edge spectra of *Eucalyptus* exudates exhibit an intense peak centered at 287.4 eV assigned to 1s–π^* transitions in phenolic groups (Ar–OH) (35) (Fig. 1*C* and *SI Appendix*, Table S6). The presence of OH groups is confirmed by the FT-IR band at 3,326 cm^{-1} (O–H stretching) (*SI Appendix*, Fig. S3*A*) and by the bands centered at 1,340 and 1,200 cm^{-1} attributed to the OH deformation/C–OH stretching in O–H (*SI Appendix*, Fig. S3*C*). The presence of aromatic groups is noticeable by the bands at 1,612, 1,534, and 1,447 cm^{-1} (C=C stretching in aromatic groups) (*SI Appendix*, Fig. S3*C*). The electronic transitions at 287.4 eV could have been as well attributed to 1s–3p/σ^* transitions in aliphatic (C_xH_y) groups; however, the lack of intense FT-IR bands in the region 3,000 to 2,800 cm^{-1} confirms the absence of CH_2 and CH_3 groups (only a weak aliphatic signal can be seen for *Eucalyptus largiflorens*) (*SI Appendix*, Fig. S3*B*).

White mallee and *E. largiflorens* spectra are characterized by the presence of 1s–π^* transitions in aromatic rather than olefinic carbon (centered at 285.5 and 285.6 eV, respectively) (Fig. 1*C*). This is confirmed by the presence of FT-IR bands at 1,612, 1,534, and 1,447 cm^{-1} attributed to the C=C stretching in aromatic compounds (*SI Appendix*, Fig. S3*C*). The polyphenolic nature of *Eucalyptus* species is confirmed by the chromatographic-mass spectrometric data: the pyrogram of white mallee is dominated by the signal of the methylated derivative of gallic acid (3,4,5-trihydroxybenzoic acid), while the most abundant peaks in the pyrogram of *E. largiflorens* are the methylated derivatives of gallic acid and other phenolic compounds, including 1,3,5-trimethoxybenzene and 1,3,5-trimethoxy-2-methyl-benzene (*SI Appendix*, Fig. S11). Gallic acid derives from hydrolyzable tannins, where it is linked via ester bonds to a core polyol, mostly glucose, in a variety of complex structures (33) (*SI Appendix*, Figs. S11 and S12). In *E. largiflorens*, in addition to hydrolyzable tannins, relatively high amounts of condensed tannins are present, which is evident by the detection of other aromatic phenols. Condensed tannins are oligomers and polymers derived from polyhydroxyflavan-3-ols linked via carbon–carbon bonds between the flavanol subunits (33). The pyrolysis in the presence of TMAH is very likely to produce variably substituted polyphenols (*SI Appendix*, Fig. S12).

The main differences between *Eucalyptus* species is the intensity of the XRS features corresponding to the presence of carboxyls (–COOH) and aliphatic alcohols (R–OH) (Fig. 1*C*). The 1s–π^* transitions in carboxyls centered at 288.5 eV are higher for the white mallee species, which agrees with the higher intensity of the band at 1,700 cm^{-1} in the FT-IR spectra attributed to C=O stretching (*SI Appendix*, Fig. S3*A*). At the XRS oxygen K-edge, white mallee exhibits a higher intensity π^* resonance centered at 532.1 eV attributed to oxygen 1s–π^* transitions in carboxyls (–COOH) (*SI Appendix*, Fig. S2*C*). This is in agreement with the higher content of hydrolyzable tannins in white mallee and thus its higher content in gallic acid (*SI Appendix*, Fig. S11). The feature at 535.2 eV is attributed to the O–H oxygen 1s–π^* transitions in carboxyl groups.

The XRS feature centered at 289.4 eV, attributed to the 1s–3p/σ^* electronic transitions in aliphatic alcohols (R–OH), is more intense for *E. largiflorens* species (Fig. 1*C* and *SI Appendix*, Table S6). The higher abundance of aliphatic hydroxyl groups in *E. largiflorens* is justified by the higher content in condensed tannins, bearing an OH group in position 3 of each flavan unit. Both *Eucalyptus* species lack intense bands around 2,900 cm^{-1}; only weak intensity peaks at 2,977 and 2,934 cm^{-1} are present in the spectra of *E. largiflorens* (*SI Appendix*, Fig. S3*B*). This suggests a low proportion of C–H bonds compared to C–C/C=C/C≡C bonds (substituted or fused cycloalkanes and unsaturations). In addition, FT-IR data suggest a higher proportion of carbohydrates in *E. largiflorens*. These data are in agreement with the Py-GC-MS data: sugars are detected in the pyrograms in the form of variably methylated 3,6-deoxy-hexonic acid methyl esters (40). These are well visible in the chromatographic profile obtained from *E. largiflorens* and only present in trace amounts of *Eucalyptus* white mallee (*SI Appendix*, Fig. S11). Sugars are linked via ester bonds to gallic acid in hydrolyzable tannins (40).

***Acacia* Gums.** *Acacia* gums are polysaccharide gums, based on arabinose, rhamnose, glucuronic acid, and galactose (*SI Appendix*, Fig. S14 and Table S7). The XRS spectra of *Acacia* exhibit significant spectral differences among the two species (Fig. 1*D* and *SI Appendix*, Table S6); the abundance of the various peaks is

Downloaded from https://www.pnas.org by 82.142.7.94 on May 26, 2022 from IP address 82.142.7.94.

different, and the varied center of the fitted Gaussians in the same energy transfer region indicates differences in chemical composition (*SI Appendix*, Table S4). The sample of unknown *Acacia* species lacks the aromatic and/or olefinic carbon (no feature around 285.4 eV) and exhibits an intense feature centered at 289.6 eV which corresponds to the 1s–3p/σ^* transitions in hydroxyls (R–OH) (Fig. 1*D*). The intense FT-IR band centered at 3,410 cm^{-1}, present in both samples, is attributed to the O–H stretching (*SI Appendix*, Fig. S3*A*).

Acacia sp. exhibits a small feature in the XRS carbon K-edge spectrum centered at 286.8 eV attributed to the 1s–π^* transitions in ether groups (R–O–R′) (Fig. 1*D*) (41, 42). The shoulder centered at 288.6 eV is attributed to the 1s–π^* in acetal carbons [$R_2C(OR')_2$] (41–43). Compared to *Acacia* sp., *Acacia bakeri* exhibits higher-intensity peaks centered at 286.8 eV attributed to the 1s–π^* transitions in ether groups (R–O–R′) (Fig. 1*D* and *SI Appendix*, Table S6) (41, 42) and at 288.6 eV attributed to the 1s–π^* of acetal carbons [$R_2C(OR')_2$] (Fig. 1*D* and *SI Appendix*, Table S6, Gaussians 3 and 5) (41–43). O–C–O carbon is considered highly diagnostic for sugars since it can be found in a limited number of organic compounds (44). For *A. bakeri*, the XRS feature centered at 290.6 eV indicates the presence of alkyl groups (Fig. 1*D*). XRS emphasizes the presence of aromatic and/or olefinic carbon solely in *A. bakeri* (Fig. 1*D*). The XRS carbon K-edge spectrum of *A. bakeri* exhibits a peak at 285.3 eV attributed to 1s–π^* transitions in aromatic and/or olefinic carbon.

The FT-IR spectra of *Acacia* species (*A. bakeri* and *Acacia* sp.) exhibit the following features (*SI Appendix*, Fig. S3): 1) an intense broad band in the 3,600 to 3,000 cm^{-1} range attributed to O–H stretching, 2) a peak centered at 2,940 cm^{-1} attributed to the CH_2 antisymmetric stretching and a band at 2,890 cm^{-1} linked to the CH stretching, 3) a broad asymmetrical band centered at 1,609 cm^{-1} possibly linked with the presence of absorbed water, 4) two intense bands at 1,420 and 1,380 cm^{-1} possibly attributed to the deformation of CH_3 and CH_2 groups, and 5) a broad band centered around 1,070 cm^{-1} and two bands centered at 1,160 and 1,130 cm^{-1} linked to the skeletal vibrations of polysaccharides.

The spectral data are in agreement with the polysaccharide nature of the two gums. The main difference among them is the fact that *Acacia* sp. has a relatively higher content of hydroxyl groups and that *A. bakeri* presents a relatively higher content of acetal and ether groups. This could be related to the fact that *Acacia* sp. contains inositol (*SI Appendix*, Fig. S14), which only presents OH groups and no ether nor acetal groups. A higher content of ether groups in *A. bakeri* is possibly due to the fact that the polysaccharide in this gum is more branched than in *Acacia* sp. as one ether bond is produced upon formation of each glycosidic bond, while the number of acetal groups remains unvaried. For *A. bakeri* the ratio of the fitted Gaussian distribution integrated area at 286.8 eV (ether groups) to the fitted Gaussian distribution integrated area at 288.6 eV (acetal groups) ($A_{fit}^{ether}/A_{fit}^{acetal} = 1.46$) is higher compared to the *Acacia* sp. ($A_{fit}^{ether}/A_{fit}^{acetal} = 0.21$), which confirms the higher branching of the former (*SI Appendix*, Table S6). Another difference among the gums is that *A. bakeri* presents aromatic–olefinic carbons, which are not found in *Acacia* sp.; such aromatic fraction is not visible by the GC-MS approach used.

XRS as an Unconventional Complement to FT-IR and GC-MS Analysis

We show that XRS offers a powerful approach to determine the fundamental composition of these complex organic cultural materials. The historical collection provides an opportunity to understand the chemical nature of the plant exudates that have undergone aging processes for over a century; samples within the collection kept at simultaneous, yet unknown conditions. This work demonstrates the advantage of XRS in the characterization of inherently complex natural materials, composed of a variety of classes of organic molecules. Synchrotron-based XANES spectroscopy yields powerful element specific information about the chemical speciation of materials, including its structure, bond distances, and configurations (22). For light elements such as carbon, K-edge XANES is conventionally performed with soft X-rays (280 to 350 eV). Soft X-rays have a very short penetration depth due to their stronger interaction with matter, which makes them a powerful surface science probe. However, this property imposes stringent constraints on sample type, preparation, and analytical environment. The need to keep the object of study under ambient pressure and temperature precludes the use of soft X-ray techniques for noninvasive studies of most precious or rare materials. On the contrary, XRS is a hard X-ray probe which, to first approximation, has the same spectral information as XANES. The energy transfer in XRS corresponds to the incident X-ray energy in XANES. With the availability of powerful synchrotron sources and efficient new X-ray spectrometers (45–48), the application of XRS as a bulk-sensitive probe of light elements has burgeoned (49–52). Recently, XRS has been applied to probe the carbon speciation in paleontological specimens (23, 24, 53).

Chromatographic–mass spectrometric techniques allow the separation and identification of characteristic marker compounds in complex organic matrices with a high degree of sensitivity and specificity (54, 55). However, they require removing a sample from the object, of at least few tens of micrograms (bulk analysis), which is always a limitation when dealing with the study of important cultural and historical samples. Analytical pyrolysis entails the reconstruction of the organic chemical composition of a sample—including amorphous, insoluble, and nonhydrolyzable polymers—based on the recognition of its thermal degradative profile (56). The connection between the chemical composition of a material and its thermal degradation products is not necessarily straightforward, nor always possible. GC-MS determines the organic chemical composition of a complex natural material after chemical workup, such as hydrolysis and derivatization procedures, which are specific for each class of material (54). Insoluble and nonhydrolyzable polymers cannot be analyzed by GC-MS alone. XRS, however, gives bulk information on all the fractions of a material, from the volatile fraction to the amorphous, insoluble, and nonhydrolyzable polymer, without any thermal nor chemical pretreatment and thus without preparation affecting the sample molecular features.

ATR-FTIR and optical Raman can be carried out noninvasively. Besides probing a different aspect of the chemical structure (vibrational excitations) (57–60), the probe depth of both techniques is three orders of magnitude shorter (approximately micrometers) than that of XRS (approximately millimeters to centimeters). XRS provides bulk sensitivity, with no or very little impact from surface alteration and contamination, which is a major advantage when studying altered biological systems. ATR-FTIR requires contact of the crystal with the sample, which may cause deformation. The recognition of minor components might not be possible with FT-IR, due to band superimposition. In optical Raman analysis of organic compounds, electronic transitions may be activated producing fluorescence phenomena that decrease signal sensitivity. These undesired phenomena led to the development of surface-enhanced Raman scattering that quenches fluorescence and increases Raman signal but requires invasive

Downloaded from https://www.pnas.org by 82.142.7.94 on May 26, 2022 from IP address 82.142.7.94.

sample treatment (61). XRS is a noninvasive technique; however, it requires access to a synchrotron and to an XRS spectrometer.

Classification of Compounds into Chemical Classes

Among the objectives of the study was to provide a spectral signature for each exudate, which carries information on its bonding structure. We have applied Fisher's linear discriminant analysis (LDA), a supervised statistical learning algorithm, to examine if the multivariate decomposition of the XRS signal (*SI Appendix*, Table S6) carries enough information to discriminate between the various genera. LDA was applied to the data consisting of the integrated area of the fitted Gaussian distributions in the energy transfer region 283.0 to 290.5 eV. For a sample set consisting of K classes (here $k = 4$), LDA is proposing $K - 1$ orthogonal projections such that the between-group scatter is maximal with respect to the within-group scatter. Following this criterion, the first projection, also termed first component of the LDA, is best discriminating each of the K classes, the second projection is optimal when the data are projected on the hyperplane orthogonal to first projection, and so on. Fig. 3*A* represents the results of the LDA applied to the XRS data. In this graph, there is a clear separation between the data points of each genus, supporting the capacity of the XRS data to discriminate the genus of sample of unknown origin. To further assess the discriminating power of the XRS decomposed spectra, we tested the hypothesis that the separation seen on the LDA is obtained by mere chance through overfitting of the data, a not so unlikely possibility since we are analyzing only eight samples for $k = 4$ classes and $N = 7$ variables. To test this hypothesis we took an original combinatorial approach (detailed in *SI Appendix*), which enables us to reject this hypothesis with a p-value $= 1.31\%$, below the standard 5% threshold (Fig. 3*B*).

The present multianalytical study classifies the plant exudates deriving from different native Australian genera in broader chemical classes: phenolic and aromatic compounds (*Eucalyptus* and *Xanthorrhoea*), polysaccharides (*Acacia*), and terpenoids (*Callitris*). The chemical characterization of these genera can inform on the cultural uses of the plant exudates. The chemical similarity of plant exudates unique of the ecosystem of Australia (e.g., *Callitris*) with plant exudates widely used in Europe (e.g., African sandarac [*Tetraclinis*]) highlights how cultures across the world converged toward similar solutions and the parallel uses of materials deriving from distinct plant genera. The plant exudates this study analyzed fall into the categories of two examples of resins, one of kino and one of gum, by the chemical classification.

The Australian grass tree *Xanthorrhoea* produces a resinous material dominated by aromatic and phenolic hydrocarbons including aromatic and/or olefinic carbon, consistent with their categorization as plant resins and their physical properties and use in hafting. The three *Xanthorrhoea* resins characterized in this study present very similar compositions from a qualitative point of view, although differences are observed from the quantitative point of view. Resin *X. semiplana* is the one with the highest content of flavanones and, possibly, polyflavanoids. The resins *X. tateana* and *X. arborea* present a relatively higher content of chalcones. The *Xanthorrhoea* species are unique to Australia, and the genus name *Xanthorrhoea* means "yellow flow," denoting the color of their exudates; however, when dried, the color of the brittle resin can range from yellow to red. Given their low solubility in water, Aboriginal Australians use *Xanthorrhoea* for practical purposes including hafting, waterproofing, or repair of bark containers and canoes and artistic purposes (e.g., attaching elements to objects) (62–64). *Xanthorrhoea* species are geographically well defined; thus, they can be valuable for tracing the source of the object and the exchange between communities (12). Recent Aboriginal Australian artists including Lindsay Harris, Christopher Pease, and Rover Thomas have used *Xanthorrhoea* resins in their artworks as pigment binders (13), as a choice linked to country and culture.

Callitris, a genus prominent and unique in Australian ecosystems, belongs to the chemical class of diterpenoid resins with a substantial presence of carboxylic acids, including callitrisic and isocommunic acid. Only a limited amount of literature exists on the chemistry of *Callitris* plant exudates, perhaps due to its specific geographic location. One exception is Simoneit et al. (37), who documented that the general chemistry and color of *Callitris* exudates are similar to others in the *Cupressaceae* (cypress) family including their ability to polymerize similar to exudates from other conifer tree species. The three *Callitris* resins analyzed in this study present a different composition. *C. calcarata* contain a major fraction of pimarane terpenoids and only trace amounts of abietanes. *Callitris verrucosa* presents a higher content of abietanes—callitrisic acid—and a minor content of pimaranes

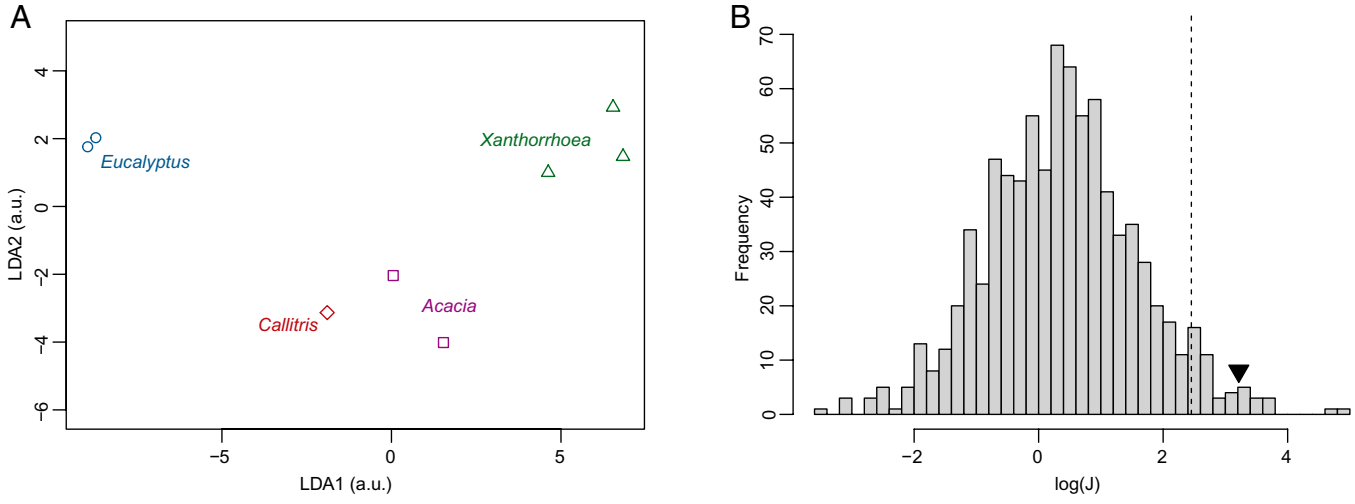

Fig. 3. Fisher's LDA. (*A*) Fisher's LDA applied to the Gaussian decomposition of the XRS spectra of eight samples of known genera. Projection on the first two (out of three) best directions found by LDA. (*B*) The histogram of log(*J*), where *J* is the metric of the LDA, for all the possible nonequivalent groupings with groups of three, two, two, and one samples. The vertical dashed line represents the 5% *p*-value threshold of these statistics, and the black triangle represents the value of log(*J*) obtained for the grouping based on the genera of the samples.

Downloaded from https://www.pnas.org by 82.142.7.94 on May 26, 2022 from IP address 82.142.7.94.

(mainly isopimaric acid). *Callitris glauca* has comparable amounts of pimaranes (sandaracopimaric and isopimaric acids) and abietanes (callitrisic acid). Abietane and pimarane terpenoids are common constituents of other terpenoid resins, including those from *Pinus* spp., *Larix* spp., and *Abies* spp. commonly used in the formulation of pictorial varnishes (65). The three *Callitris* resins analyzed in the current study contain also labdane diterpenoids, which produce a polymeric fraction—polycommunic acid—which is also found in African sandarac (*Tetraclinis*), a well-studied resin widely used as varnish in European artworks (39, 66). Similarly to the *Xanthorrhoea* exudates, *Callitris* are also resins and therefore can used in binding and adhesives (6). Many European historical manuscripts describe recipes of varnishes made with sandarac and highlight its use as a high-quality material (67–70). Although *Callitris* was also used as a varnish, it has not been extensively exported from Australia (66).

Eucalyptus exudates are primarily dominated by phenolic and other aromatic constituents. In the literature, exudates from *Eucalyptus* species are often described as gums or resins (e.g., "gum tree"). This terminology can be misleading since they are neither polysaccharide nor terpenoid; rather, they are more accurately described as kino, which is chemically defined by Lambert et al. as dominated by phenolic and other aromatic constituents (71, 72). Kino composition is based on the presence of hydrolyzable tannins (gallic acid and sugars) and condensed tannins (poly hydroxyflavan-3-ols) which creates the significant tannin composition of the kino, and it is at the base of its characteristic astringent properties (33). The two *Eucalyptus* kinos analyzed in this study presented quite different compositions. White mallee is mainly constituted by hydrolyzable tannins, with a relatively low content of sugars. *E. largiflorens* comprises relatively high amounts of both hydrolyzable tannins (with a higher sugar content) and condensed tannins. In general the liquid exudate hardens in air, and the kinos can be categorized generally into groups based on their solubilities in alcohol and water. Colors of *Eucalyptus* kino range from dark red-brown to yellow and range from very friable to breaking into large fragments (73). Kino was used by Aboriginal Australian peoples for medical applications including treating wounds and tooth decay, for infections, colds and influenza, and as an astringent, and continues to have applications today (11, 73).

Acacia exhibit characteristic features of polysaccharides; thus, they belong to the wide category of gums. As such, they are water-soluble materials that contain polysaccharide–protein complexes and are biopolymers which can act as emulsifiers that occur in a range of colors (74). Stretching back 70,000 y ago, *Acacia* has found many applications in arts, cosmetics, medicines, and food and continues to be a significantly traded commodity worldwide (74). Aboriginal Australian peoples use acacia (wattle gum) in a variety of food preparations, either by mixing the gum in water or mixing with other native foods such as eugenia apples, as well as in medicinal preparations for treating colds and coughs (11, 75–77). In arts, *Acacia* gums are found as binders across several cultures for various painting and ink media (e.g., watercolors and gouache) (74, 78, 79). Gum Arabic, one of the most notable gums historically used as binding media in artworks across Africa, the Mediterranean region, and Asia, derives from *A. senegal* and *Acacia seyal* (recently named genera *Senegalia* and *Vachellia*, respectively), and it is harvested commercially mainly in Sudan (80%) (1). Although the majority of the species of *Acacia* are in Australia, the majority of the analyses have focused on the commercial species *S. senegal* and *V. seyal*.

The *Acacia* gums analyzed in this study present a saccharide-composition which is very similar to that of other gums from African Acacia species (80), especially that of *S. senegal*, as shown in *SI Appendix*, Table S7.

Cultural Uses and Limitation of Extant Data

Cultural heritage conservators often face the challenge of treating an object while respecting the artistic intent and cultural factors, thus avoiding interventions with modern synthetic materials where possible (81). The accurate characterization and understanding of the natural binders' chemical and physical properties and stability are important for the treatment decisions as well as understanding the intent of the artist. There is extensive literature on the analysis of European artists' binder materials across several categories including resins, polysaccharides, terpenoids, waxes, and oils (10); however, the characterization of native Australian materials is significantly understudied as compared to European materials. In addition, there are not complete or comprehensive datasets for Australian raw materials, as there are for European, Asian, African, and North and South American materials [see, for instance, the Infrared and Raman Users Group database (82)]. Therefore, this work contributes to our fundamental understanding of Australian plant exudates and, crucially, provides a reliable method for identification and differentiation of traditional binders in museum, art gallery, and cultural collections (13).

Conclusion

We have demonstrated the complementary use of XRS, FT-IR, and GC-MS to analyze a unique historical collection and successfully identified key genera-specific chemical features for native Australian plant exudates. XRS elucidates the fundamental bonding information of light elements, FT-IR reveals the functional group information, and GC-MS provides information about the molecular structure through characterization of the molecular pattern obtained after thermal degradation or chemical workup. The fundamental chemistry and material properties of the exudates often shape their cultural use; therefore, it is no surprise that natural materials utilized over thousands of years of tradition continue to inspire their present and future uses. The combination of these techniques delivers a powerful characterization and chemical classification of bulk plant exudates and their properties with further potential for identification in artworks, cultural heritage items, and museum collections.

Materials and Methods

Materials. A sample set of native Australian plant genera (*Eucalyptus*, *Callitris*, *Xanthorrhoea*, and *Acacia*), summarized in *SI Appendix*, Table S1, were analyzed. The samples were selected from SAM collections and a historical biological collection gathered from diverse locations across Australia and held for years in the South Australia state forensic laboratory and are now located at Flinders University. Unfortunately, the collectors of this exceptional comprehensive collection are unknown, and the original data notebooks no longer exist; however, samples in the historical biological collection are over a century old, where each amber jar is clearly labeled with the collection location and date, and the samples offer an unprecedented study set. While the exact storage conditions are unknown across time, they are consistent within the collection, which minimizes the effects of variables such as temperature and humidity.

XRS Spectroscopy. X-ray Raman measurements (carbon K-edge) were performed using the high-resolution X-ray Raman spectrometer operated at beamline 6-2 at the Stanford Synchrotron Radiation Laboratory (46). The instrument consists of 40 crystal Si(440) analyzers arranged on overlapping Rowland circles of 1,000 mm and at a fixed Bragg angle of 88°, resulting in a fixed detection energy at 6,462 eV and an overall energy resolution of 0.29 eV. Spectra are

Downloaded from https://www.pnas.org by 82.142.7.94 on May 26, 2022 from IP address 82.142.7.94.

recorded using an inverse scanning approach, wherein the detection energy is held constant while the incident energy is scanned through a Si(311) double-crystal monochromator. The average momentum transfer is $q \approx 0.65$ Å^{-1}, which ensures that dipole transitions dominate the spectra, and therefore, the X-ray Raman spectra are formally equivalent to conventional soft X-ray absorption spectra. A detailed description of the XRS data reduction procedure is documented in *SI Appendix*.

Statistical Testing of XRS Data Classification. Fisher linear discrimination is finding the projections that maximize the ratio J of the between-group scatter divided by the within-group scatter. Formally, for a given set of projections defined by their matrix $\mathbf{W}$, noting $\mathbf{S}_B$ and $\mathbf{S}_W$ as the between-group and within-group scatter matrices, respectively, and for any square matrix $\mathbf{M}$ noting $|\mathbf{M}|$ as its determinant, J is defined by

$$J(\mathbf{W}) = \frac{|\mathbf{W}^t \mathbf{S}_B \mathbf{W}|}{|\mathbf{W}^t \mathbf{S}_W \mathbf{W}|}.$$

To assess the quality of the discrimination obtained based on the genera of the samples, we compared the value of J with the one obtained for all other possible (random) grouping of the samples with the same group sizes. A detailed description of the statistical testing of XRS data classification is documented in *SI Appendix*.

FT-IR. FT-IR spectra were collected with a spectrometer Bruker Alpha II equipped with a DLATGS (Deuterated L-Alanine Triglycine Sulphate) detector. Measurements were performed in transmission mode using KBr pellets (Sigma Aldrich, FT-IR grade, ref. 221864). A total of 128 scans have been accumulated in each sample, using a resolution of 4 cm^{-1} in the range between 4,000 and 400 cm^{-1}. All spectra shown have not been corrected in order to avoid any kind of distortion.

Py-GC-MS. Py-GC-MS experiments were performed at Flinders University, using a Frontier Laboratories Single-Shot pyrolyzer PY-3030S-220 (Shimadzu North America) coupled to an Agilent Technologies 7890A GC System (Agilent Technologies) with an Agilent Technologies 5975C inert XL electron impact/chemical ionization mass-selective triple axis detector (Agilent Technologies). The sample preparation procedures followed Reeves et al. (10), with preparation of the samples using in situ thermally assisted hydrolysis and methylation with TMAH.

GC-MS. The analytical procedure used was adapted from a work previously published (81) and is based on the acidic hydrolysis of the sample assisted by microwaves, followed by derivatization of sugars to produce diethyl-dithioacetal trimethylsilyl derivatives and GC-MS analysis. Details of the analytical procedure and instrumental parameters are reported in *SI Appendix*.

Data Availability. Analytical data have been deposited in Zenodo (DOI: 10.5281/zenodo.5484203) (83).

ACKNOWLEDGMENTS. We are grateful for various researchers originating and maintaining the samples over the decades. We are grateful for access to the historical collection and use of samples from the SAM. We acknowledge the Indigenous lands where the samples originated. We acknowledge the SOLEIL and SSRL synchrotrons for the provision of beamtime. U.B. and L.B. acknowledge support from the France–Stanford Center for Interdisciplinary Studies Program and the LabEx Patrimoines matériels: savoirs, patrimonialisation, transmission (PATRIMA, Agence Nationale de la Recherche, 10-LABX-0094)/Fondation des Sciences du Patrimoine for U.B.'s invited professorship at Université Paris-Saclay. R.S.P.-F. acknowledges the Flinders University Outside Studies Program and the Australian Synchrotron International Synchrotron Access Program for a research visit to Stanford University. We thank Alessia Andreotti from the Department of Chemistry and Industrial Chemistry of the University of Pisa for her help with the GC-MS analysis of polysaccharide gums. R.G.'s PhD work was funded by Université de Versailles – Saint-Quentin-en-Yvelines and Synchrotron SOLEIL. R.G. acknowledges support from Université Paris-Saclay for the financing of a visit to Stanford. R.G. acknowledges support from the State Scholarships Foundation of Cyprus for doctoral studies. Portions of this research were carried out at the Stanford Synchrotron Radiation Lightsource, a national user facility operated by Stanford University on behalf of the US Department of Energy, Office of Basic Energy Sciences, and we thank the user support staff at SSRL.

Author affiliations: [a]Université Paris-Saclay, CNRS, Ministère de la Culture, UVSQ, MNHN, IPANEMA, F-91192 Saint-Aubin, France; [b]Synchrotron SOLEIL, F-91192 Gif-sur-Yvette, France; [c]School of Geography, Earth and Atmospheric Sciences, University of Melbourne, Melbourne, VIC, Australia 3010; [d]College of Science and Engineering, Flinders University, Adelaide, SA, Australia 5001; [e]Stanford Synchrotron Radiation Lightsource, SLAC National Accelerator Laboratory, Menlo Park, CA 94025; [f]AXES Research Group, NanoLab Center of Excellence, University of Antwerp, 2020 Antwerp, Belgium; [g]Department of Chemistry and Industrial Chemistry, University of Pisa, I-56124 Pisa, Italy; [h]Muséum National d'Histoire Naturelle, Sorbonne Université, CNRS, UMR 7590, Institut de Minéralogie, Physique des Matériaux et Cosmochimie, Paris, France; [i]Laboratoire de Chimie Physique-Matière et Rayonnement, Sorbonne Université, CNRS, 75005 Paris, France; [j]Stanford PULSE Institute, SLAC National Accelerator Laboratory, Menlo Park, CA 94025; [k]Department of Physics, University of Wisconsin–Madison, Madison, WI 53706; and [l]Université Paris-Saclay, ENS Paris-Saclay, CNRS, PPSM, 91190 Gif-sur-Yvette, France

Author contributions: R.S.P.-F., U.B., and L.B. designed research; R.G., D.S., V.B., I.B., J.S., R.L., S.B., J.-P.R., and L.B. performed research; D.S. and J.-P.R. contributed new reagents/analytic tools; R.G., D.S., V.B., I.B., J.S., S.X.C., R.L., J.-P.R., and L.B. analyzed data; R.G., V.B., I.B., J.S., R.L., J.-P.R., U.B., and L.B. interpreted data; R.G. and S.X.C. performed statistical analysis; S.B. reviewed the assignment of X-ray Raman spectroscopy features; and R.G., R.S.P.-F., U.B., and L.B. wrote the paper.

The authors declare no competing interest.

This article is a PNAS Direct Submission. C.P. is a guest editor invited by the Editorial Board.

1. A. Nussinovitch, *Plant Gum Exudates of the World: Sources, Distribution, Properties, and Applications* (CRC Press, Boca Raton, FL, 2010).
2. A. P. Rauter, F. B. Palma, J. Justino, M. E. Araújo, S. P. dos Santos, *Natural Products in the New Millennium: Prospects and Industrial Application* (Springer Science & Business Media, 2013), **vol. 47**.
3. C. Mantell, The natural hard resins–Their botany, sources and utilization. *Econ. Bot.* **4**, 203–242 (1950).
4. Z. Cumpston, Food, tools and medicine: 5 native plants that illuminate deep Aboriginal knowledge (2020). https://theconversation.com/food-tools-and-medicine-5-native-plants-that-illuminate-deep-aboriginal-knowledge-145240. Accessed 31 August 2021.
5. A. J. Blee, K. Walshe, A. Pring, J. S. Quinton, C. E. Lenehan, Towards the identification of plant and animal binders on Australian stone knives. *Talanta* **82**, 745–750 (2010).
6. C. Matheson, A. McCollum, Characterising native plant resins from Australian Aboriginal artefacts using ATR-FTIR and GC/MS. *J. Archaeol. Sci.* **52**, 116–128 (2014).
7. J. F. Parr, The identification of Xanthorrhoea resins by starch morphology: Prospects for archaeological and taxonomic applications. *Econ. Bot.* **56**, 260–270 (2002).
8. J. Parr, Once, twice maybe, but not three times: Reheating *Xanthorrhoea australis* resin. *Aust. Archaeol.* **49**, 23–27 (1999).
9. O. Powell, R. J. Fensham, P. Memmott, Indigenous use of spinifex resin for hafting in north-eastern Australia. *Econ. Bot.* **67**, 210–224 (2013).
10. T. Reeves, R. S. Popelka-Filcoff, C. E. Lenehan, Towards identification of traditional European and Indigenous Australian paint binders using pyrolysis gas chromatography mass spectrometry. *Anal. Chim. Acta* **803**, 194–203 (2013).
11. P. A. Clarke, *Aboriginal People and Their Plants* (Rosenberg Publishing, Dural, Australia, 2011).
12. F. Bradshaw, Chemical characterisation of museum-curated ethnographic resins from Australia and New Guinea used as adhesives, medicines and narcotics. *Herit. Sci.* **1**, 36 (2013).
13. S. Alcock, Painting Country: Australian Aboriginal artists' approach to traditional materials in a modern context. *AICCM Bull* **34**, 66–74 (2013).
14. T. Maloney, R. Wood, S. O'Connor, R. Whitau, Direct dating of resin hafted point technology in Australia. *Aust. Archaeol.* **81**, 35–43 (2015).
15. N. M. Smith, Ethnobotanical field notes from the Northern Territory, Australia. *J. Adel. Bot. Gard.* **14**, 1–65 (1991).
16. D. Gilroy, I. Godfrey, Conservation and care of collections–Bark paintings (2017). https://manual.museum.wa.gov.au/conservation-and-care-collections-2017/ethnographic-material/bark-paintings. Accessed 31 August 2021.
17. B. Tworek-Matuszkiewicz, Australian Aboriginal bark paintings – their history, structure and conservation. *Stud. Conserv.* **52**(1), 15–28 (2007).
18. A. H. Thornhill *et al.*, A dated molecular perspective of eucalypt taxonomy, evolution and diversification. *Aust. Syst. Bot.* **32**, 29–48 (2019).
19. G. F. Smith, E. Figueiredo, Conserving *Acacia* Mill. with a conserved type: What happened in Melbourne? *Taxon* **60**, 1504–1506 (2011).
20. U. Bergmann, P. Glatzel, S. P. Cramer, Bulk-sensitive XAS characterization of light elements: From X-ray Raman scattering to X-ray Raman spectroscopy. *Microchem. J.* **71**, 221–230 (2002).
21. W. Schülke, *Electron Dynamics by Inelastic X-Ray Scattering* (Oxford University Press, Oxford, United Kingdom, 2007), **vol. 7**.
22. J. Stöhr, *NEXAFS Spectroscopy* (Springer Science & Business Media, 2013), **vol. 25**.
23. P. Gueriau *et al.*, Noninvasive synchrotron-based x-ray Raman scattering discriminates carbonaceous compounds in ancient and historical materials. *Anal. Chem.* **89**, 10819–10826 (2017).
24. R. Georgiou *et al.*, Carbon speciation in organic fossils using 2D to 3D x-ray Raman multispectral imaging. *Sci. Adv.* **5**, eaaw5019 (2019).
25. Y. Mizuno, Y. Ohmura, Theory of X-ray Raman scattering. *J. Phys. Soc. Jpn.* **22**, 445–449 (1967).
26. T. Suzuki, X-ray Raman scattering experiment. I. *J. Phys. Soc. Jpn.* **22**, 1139–1150 (1967).
27. A. Hitchcock, D. Mancini. Bibliography and database of inner shell excitation spectra of gas phase atoms and molecules. *J. Electron Spectrosc. Relat. Phenom.* **67**, 1–12 (1994).
28. J. B. Lambert, *Organic Structural Spectroscopy* (Pearson College Division, 1998).

Downloaded from https://www.pnas.org by 82.142.7.94 on May 26, 2022 from IP address 82.142.7.94.

29. L. Bellamy, *The Infrared Spectra of Complex Molecules* (Springer Science & Business Media, 2013).
30. D. Lin-Vien, N. B. Colthup, W. G. Fateley, J. G. Grasselli, *The Handbook of Infrared and Raman Characteristic Frequencies of Organic Molecules* (Elsevier, 1991).
31. H. Duewell, Chemotaxonomy of the genus *Xanthorrhoea*. *Biochem. Syst. Ecol.* **25**, 717–738 (1997).
32. A. Birch, C. Dahl, Some constituents of the resins of *Xanthorrhoea preissii*, *australis* and *hastile*. *Aust. J. Chem.* **27**, 331–334 (1974).
33. S. von Martius, K. A. Hammer, C. Locher, Chemical characteristics and antimicrobial effects of some *Eucalyptus kinos*. *J. Ethnopharmacol.* **144**, 293–299 (2012).
34. P. Schofield, D. Mbugua, A. Pell, Analysis of condensed tannins: A review. *Anim. Feed Sci. Technol.* **91**, 21–40 (2001).
35. J. Alleon *et al.*, Organic molecular heterogeneities can withstand diagenesis. *Sci. Rep.* **7**, 1508 (2017).
36. T. Kolev, Vibrational assignment of in-and out-of-plane modes of some aromatic and arylaliphatic ketones. *J. Mol. Struct.* **349**, 381–384 (1995).
37. B. R. T. Simoneit, R. E. Cox, D. R. Oros, A. Otto, Terpenoid compositions of resins from *Callitris* species (Cupressaceae). *Molecules* **23**, 3384 (2018).
38. Y. Zubavichus, A. Shaporenko, M. Grunze, M. Zharnikov, Innershell absorption spectroscopy of amino acids at all relevant absorption edges. *J. Phys. Chem. A* **109**, 6998–7000 (2005).
39. D. Scalarone, M. Lazzari, O. Chiantore, Ageing behaviour and analytical pyrolysis characterisation of diterpenic resins used as art materials: Manila copal and sandarac. *J. Anal. Appl. Pyrolysis* **68**, 115–136 (2003).
40. C. Riedo, D. Scalarone, O. Chiantore, Advances in identification of plant gums in cultural heritage by thermally assisted hydrolysis and methylation. *Anal. Bioanal. Chem.* **396**, 1559–1569 (2010).
41. L. S. Johansson, J. Campbell, Reproducible XPS on biopolymers: Cellulose studies. *Surf. Interface Anal.* **36**, 1018–1022 (2004).
42. V. Rouchon, S. Bernard, Mapping iron gall ink penetration within paper fibres using scanning transmission X-ray microscopy. *J. Anal. At. Spectrom.* **30**, 635–641 (2015).
43. C. Le Guillou, S. Bernard, F. De la Pena, Y. Le Brech, XANES-based quantification of carbon functional group concentrations. *Anal. Chem.* **90**, 8379–8386 (2018).
44. J. B. Lambert, Y. Wu, J. A. Santiago-Blay, Taxonomic and chemical relationships revealed by nuclear magnetic resonance spectra of plant exudates. *J. Nat. Prod.* **68**, 635–648 (2005).
45. D. Sokaras *et al.*, A high resolution and large solid angle x-ray Raman spectroscopy end-station at the Stanford Synchrotron Radiation Lightsource. *Rev. Sci. Instrum.* **83**, 043112 (2012).
46. S. Huotari *et al.*, A large-solid-angle X-ray Raman scattering spectrometer at ID20 of the European Synchrotron Radiation Facility. *J. Synchrotron Radiat.* **24**, 521–530 (2017).
47. J. P. Rueff *et al.*, The GALAXIES beamline at the SOLEIL synchrotron: Inelastic X-ray scattering and photoelectron spectroscopy in the hard X-ray range. *J. Synchrotron Radiat.* **22**, 175–179 (2015).
48. C. Weis *et al.*, Combining X-ray K$\beta_{1,3}$, valence-to-core, and X-ray Raman spectroscopy for studying Earth materials at high pressure and temperature: The case of siderite. *J. Anal. At. Spectrom.* **34**, 384–393 (2019).
49. U. Bergmann *et al.*, Carbon K-edge X-ray Raman spectroscopy supports simple, yet powerful description of aromatic hydrocarbons and asphaltenes. *Chem. Phys. Lett.* **369**, 184–191 (2003).
50. U. Bergmann, O. C. Mullins, *Carbon X-Ray Raman Spectroscopy of PAHs and Asphaltenes in Asphaltenes, Heavy Oils, and Petroleomics* (Springer, 2007), pp. 139–155.
51. U. Boesenberg *et al.*, Electronic structure changes upon lithium intercalation into graphite–insights from ex situ and operando x-ray Raman spectroscopy. *Carbon* **143**, 371–377 (2019).
52. A. E. Pomerantz *et al.*, Electronic structure of naturally occurring aromatic carbon. *Energy Fuels* **33**, 2099–2105 (2019).
53. U. Bergmann, L. Bertrand, N. P. Edwards, P. L. Manning, R. A. Wogelius, "Chemical mapping of ancient artifacts and fossils with x-ray spectroscopy" in *Synchrotron Light Sources and Free-Electron Lasers: Accelerator Physics, Instrumentation and Science Applications*, E. Jaeschke, S. Khan, J. R. Schneider, J. B. Hastings, Eds. (Springer Nature Switzerland, 2019).
54. M. P. Colombini, A. Andreotti, I. Bonaduce, F. Modugno, E. Ribechini, Analytical strategies for characterizing organic paint media using gas chromatography/mass spectrometry. *Acc. Chem. Res.* **43**, 715–727 (2010).
55. F. Caruso *et al.*, Micro-analytical identification of the components of varnishes from South Italian historical musical instruments by PLM, ESEM–EDX, microFTIR, GC–MS, and Py–GC–MS. *Microchem. J.* **116**, 31–40 (2014).
56. I. Degano, F. Modugno, I. Bonaduce, E. Ribechini, M. P. Colombini, Recent advances in analytical pyrolysis to investigate organic materials in heritage science. *Angew. Chem. Int. Ed. Engl.* **57**, 7313–7323 (2018).
57. S. Prati, G. Sciutto, I. Bonacini, R. Mazzeo, New frontiers in application of FTIR microscopy for characterization of cultural heritage materials. *Top. Curr. Chem. (Cham)* **374**, 26 (2016).
58. M. Spring, C. Ricci, D. A. Peggie, S. G. Kazarian, ATR-FTIR imaging for the analysis of organic materials in paint cross sections: Case studies on paint samples from the National Gallery, London. *Anal. Bioanal. Chem.* **392**, 37–45 (2008).
59. P. Vandenabeele, H. G. Edwards, L. Moens, A decade of Raman spectroscopy in art and archaeology. *Chem. Rev.* **107**, 675–686 (2007).
60. M. Leona, J. Stenger, E. Ferloni, Application of surface-enhanced Raman scattering techniques to the ultrasensitive identification of natural dyes in works of art. *J. Raman Spectrosc.* **37**, 981–992 (2006).
61. N. Colthup, *Introduction to Infrared and Raman Spectroscopy* (Elsevier, 2012).
62. S. Valis, Investigation into the distortion of *Triodia* and *Xanthorrhoea* resins on Australian Aboriginal artefacts in museum collections. *AICCM Bull.* **17**, 61–74 (1991).
63. V. Rots *et al.*, Hafted tool-use experiments with Australian Aboriginal plant adhesives: Triodia spinifex, Xanthorrhoea Grass Tree and Lechenaultia divaricata Mindrie. *EXARC J.* **1** (2020).
64. Koori History–Aboriginal History of South Eastern Australia, Hard Yakka! Grass Tree Resin (*Xanthorrhoea*) (2016). https://koorihistory.com/grass-tree-resin/. Accessed 31 August 2021.
65. L. Osete-Cortina, M. T. Doménech-Carbó, Analytical characterization of diterpenoid resins present in pictorial varnishes using pyrolysis-gas chromatography-mass spectrometry with on line trimethylsilylation. *J. Chromatogr. A* **1065**, 265–278 (2005).
66. J. H. Langenheim, *Plant Resins: Chemistry, Evolution, Ecology, and Ethnobotany* (Timber Press, Oregon, 2003).
67. D. V. Thompson, *The Craftsman's Handbook: Il libro dell'arte by Cennino d'Andrea Cennini* (Dover, New York, 1954).
68. D. C. Fels, J. H. Sulkowski, R. Bedell, R. A. McClung, *Lost Secrets of Flemish Painting, Including the First Complete English Translation of the De Mayerne Manuscript, BM Sloane 2052* (Alchemist, Eijsden, The Netherlands, 2004).
69. C. L. Eastlake, *Methods and Materials of Painting of the Great Schools and Masters* (Dover, New York, 2001).
70. M. P. Merrifield, *Medieval and Renaissance Treatises on the Arts of Painting: Original Texts with English Translations* (Dover, New York, 1999).
71. J. B. Lambert, Y. Wu, M. A. Kozminski, J. A. Santiago-Blay, Characterization of Eucalyptus and chemically related exudates by nuclear magnetic resonance spectroscopy. *Aust. J. Chem.* **60**, 862–870 (2007).
72. J. B. Lambert, E. A. Heckenbach, Y. Wu, J. A. Santiago-Blay, Characterization of plant exudates by principal-component and cluster analyses with nuclear magnetic resonance variables. *J. Nat. Prod.* **73**, 1643–1648 (2010).
73. C. Locher, L. Currie, Revisiting kinos–An Australian perspective. *J. Ethnopharmacol.* **128**, 259–267 (2010).
74. C. Sanchez *et al.*, Acacia gum: History of the future. *Food Hydrocoll.* **78**, 140–160 (2018).
75. D. Jæger *et al.*, Isolation and structural characterization of echinocystic acid triterpenoid saponins from the Australian medicinal and food plant *Acacia ligulata*. *J. Nat. Prod.* **80**, 2692–2698 (2017).
76. Koori History–Aboriginal History of South Eastern Australia, Wattle (Acacia) and its many uses (2017). http://koorihistory.com/wattle/. Accessed 31 August 2021.
77. P. A. Clarke, Australian ethnobotany: An overview. *Aust. Aborig. Stud.* **2**, 21–38 (2003).
78. C. Granzotto, J. Arslanoglu, C. Rolando, C. Tokarski, Plant gum identification in historic artworks. *Sci. Rep.* **7**, 44538 (2017).
79. M. P. Colombin, A. Ceccarini, A. Carmignani, Ion chromatography characterization of polysaccharides in ancient wall paintings. *J. Chromatogr. A* **968**, 79–88 (2002).
80. A. Lluveras-Tenorio, J. Mazurek, A. Restivo, M. P. Colombini, I. Bonaduce, Analysis of plant gums and saccharide materials in paint samples: Comparison of GC-MS analytical procedures and databases. *Chem. Cent. J.* **6**, 115 (2012).
81. Australian Institute for the Conservation of Cultural Material, "Code of ethics and code of practice" (Tech. Rep., Moonah, Australia, 2002).
82. B. A. Price, B. Pretzel, S. Q. Lomax, *Infrared and Raman Users Group Spectral Database*, 2007 ed. (Infrared and Raman Users Group, Philadelphia, 2009), vol. 1 and 2. http://www.irug.org/search-spectral-database. Accessed 5 April 2022.
83. R. Georgiou et al., Dataset on the chemistry of australian plant exudates from historical collection. Zenodo. https://zenodo.org/record/5484203#.Yn6pLOjMLcs. Accessed 13 April 2022.

Downloaded from https://www.pnas.org by 82.142.7.94 on May 26, 2022 from IP address 82.142.7.94.